Current Research (2025) Newfoundland and Labrador Department of Industry, Energy and Technology Geological Survey, Report 25-1, pages 45-62

NEW GEOCHRONOLOGY DATA FROM THE REE OCCURRENCES AND ASSOCIATED ROCKS IN THE PORT HOPE SIMPSON–St. LEWIS AREA, SOUTHEASTERN LABRADOR

Z. Magyarosi and N. Rayner[1]
Mineral Deposits Section
[1]Geological Survey of Canada, Natural Resources Canada, 601 Booth Street, Ottawa, ON, K1A 0E8

ABSTRACT

Rare-earth-element (REE) occurrences in the Port Hope Simpson – St. Lewis area, located in the Grenville Province in southeastern Labrador, represent the most recently discovered Mesoproterozoic alkaline-silicate REE–HFSE system in Labrador. Rare-earth-element occurrences in the north are hosted in deformed and metamorphosed granitoids and syenite to monzonite forming an ~64-km-long belt up to 2 km in thickness (FHB–Fox Harbour Belt). In the south, REE mineralization is hosted in pegmatites associated with their parent granites and syenites (FHS–Fox Harbour South).

New geochronology results from the FHB returned ages of 1074.4 ± 9.1 Ma (sample 21ZM077A01), 1054.1 ± 9.9 Ma (sample 21ZM053A03), 1049.8 ± 9.3 (rim) and 1067 ± 13 (core) Ma (sample 21ZM061A01) and 1051.5 ± 9.6 (rim) and 1072 ± 17 (core) Ma (sample 22ZM0355A01). However, based on the oldest single analysis from the inclusion-rich cores (1344 ± 24 Ma and 1238 ± 13 Ma from samples 21ZM053A03 and 22ZM0355A01 respectively) and similarities in the geochemistry, mineralogy and mineral chemistry to the rest of FHB, they are interpreted to have crystallized ca. *1300 Ma, implying that metamorphism at* ca. *1.07–1.05 Ga resulted in profound recrystallization of the original zircon. Samples from FHS returned 1239 ± 14 Ma (core) and 1020.8 ± 11 (rim) Ma (sample 22ZM0390B01), and 1230 ± 19 (core) and 1013 ± 10 (rim) Ma (sample 22ZM0442A01). The ages in the core are interpreted as igneous crystallization ages and the ages in the rim are metamorphic/partial melting ages. The core ages overlap with igneous crystallization ages from the FHB and the current and previous studies indicate a strong genetic link between them. The core ages also suggest that these intrusions are most likely the parent intrusions of the spatially associated REE pegmatites.*

Metamorphic ages of the rim analyses range between ca. *1050 and 1075 Ma in the FHB and* ca. *1013 and 1021 Ma in the FHS. The age of the country rock analyzed along the FHB (1473 ± 13 Ma) confirms that the FHB consists of three mineralized belts separated by older rocks, which are not part of the alkaline-silicate igneous system. It also indicates a more widespread presence of Pinwarian rocks in the Mealy Mountains terrane.*

INTRODUCTION

Labrador is host to several Mesoproterozoic alkaline-silicate rare-earth-element (REE) – high-field-strength-element (HFSE) enriched systems including the Red Wine Intrusive Suite, the Flowers River Igneous Suite and the world-class Strange Lake Complex (Miller *et al.*, 1997; Crocker, 2014; Ducharme *et al.*, 2021). The REE occurrences in the Port Hope Simpson–St. Lewis area were discovered by Search Minerals Incorporated in 2010, and although actively explored, the mineralization is relatively understudied compared to the other alkaline-silicate systems in Labrador, with only one of the occurrences (Foxtrot) having been investigated in detail (Figure 1; Haley, 2014). This report summarizes new results of geochronological analyses of seven samples from the REE occurrences and the surrounding rocks, and it is part of a multi-year project funded by the Geological Survey of Newfoundland and Labrador (GSNL) and the Geological Survey of Canada (GSC) through its Targeted Geoscience Initiative (TGI) program (Magyarosi, 2022; Magyarosi and Rayner, 2023, 2024, 2025). Previous geochronology data from the study area are summarized in Table 1.

Alkaline-silicate REE–HFSE igneous systems are characterized by the presence of alkaline or peralkaline rocks, even if they are dominated by metaluminous rocks (Beard *et al.*, 2022). These systems occur in continental rift, post-collisional and intraplate tectonic settings and require low-degree, high-pressure melting, under thick continental crust,

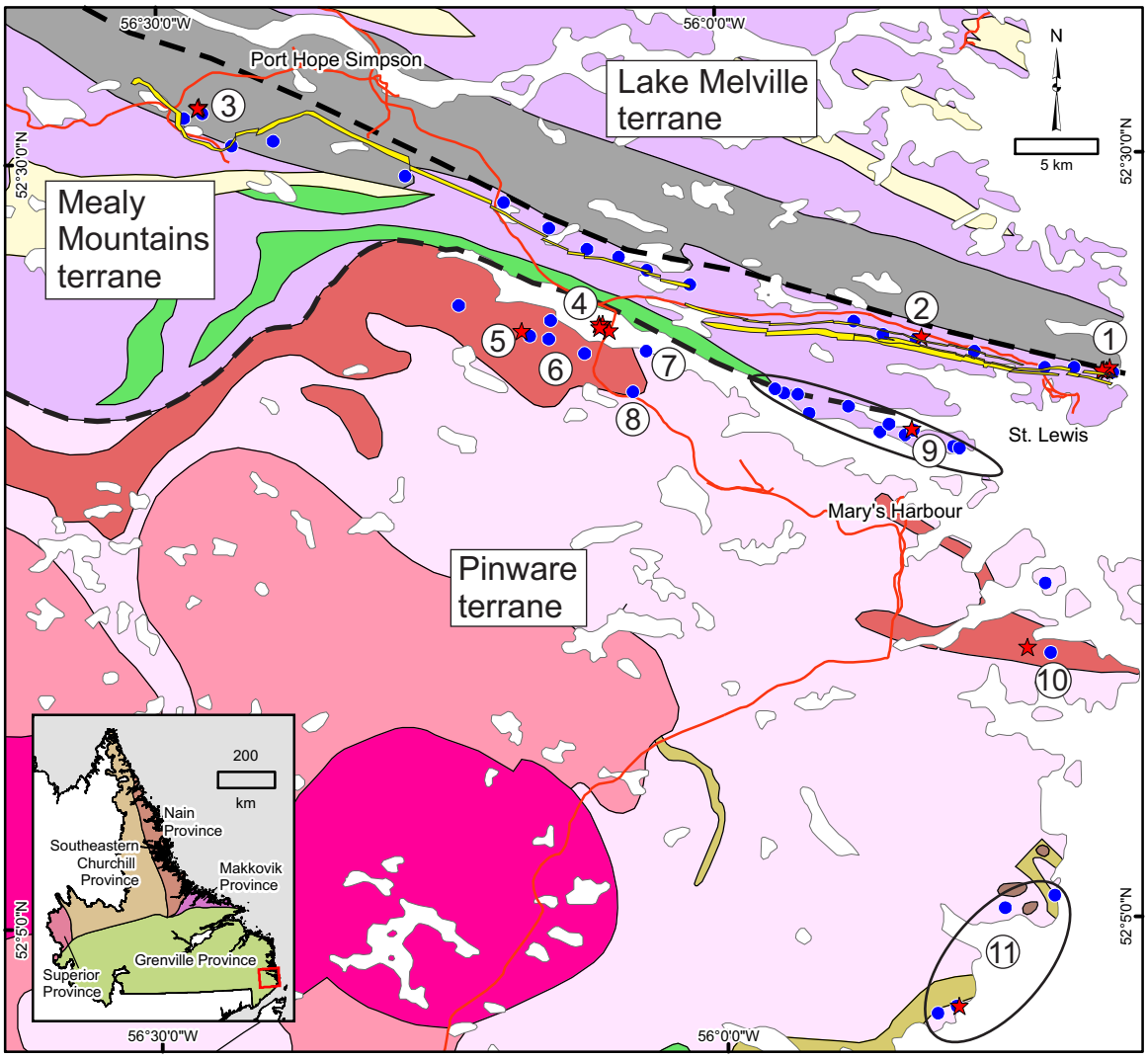

LEGEND

Phanerozoic

- NCs — Sandstone and nodular limestone; local basalt at base of sequence

Late Mesoproterozoic

- M3gr — Syenite to granite
- M3gs — Granite and syenite plutons

Early Mesoproterozoic

- M1lga — Layered gabbro-anorthosite-ultramafic intrusions

Paleo and Mesoproterozoic

- P-Mgs — Granite, syenite, monzonite, diorite and derived gneiss
- P-Msv — Metasedimentary and felsic volcanic rocks
- P-Msy — Syenite, monzonite and diorite

Late Paleoproterozoic

- P3a — Anorthosite and other mafic rocks
- P3gm — K-feldspar megacrystic granite and other granitoid plutonic rocks
- P3sgn — Pelitic, migmatitic metasedimentary gneiss and minor psammitic gneiss

SYMBOLS

- Geological contact
- Terrane boundary
- Roads
- REE mineral occurrence
- Geochronology sample
- Fox Harbour Belt

Figure 1. *Geology of the Port Hope Simpson area, southeastern Labrador (modified after Wardle* et al.*, 1997; Gower, 2010a, b, 2019). The east-northeast trending line of REE occurrences from Deep Fox (1) to Fox Meadow (3) outlines the Fox Harbour Belt mixed-classed rock unit, formerly known as the Fox Harbour Volcanic Belt. REE occurrences: 1–Deep Fox, 2–Foxtrot, 3–Fox Meadow, 4–HighREE, 5–Pesky Hill, 6–Toots Cove, 7–Southern Shore, 8–Piperstock Hill, 9–Long Point occurrences, 10–Oceanview, 11–Henley Harbour occurrences.*

Table 1. Previous U–Pb zircon geochronology data

Sample number	Lab number	Area	Lithology	Age	Interpretation	Method	Reference
21ZM065A01	12706	Deep Fox	Metaluminous granite	1065.9 ± 8.2 Ma	Metamorphism	SHRIMP	Magyarosi and Rayner (2023)
21ZM084A01	12709	Deep Fox	Metaluminous granite	1314 ± 12 Ma	Igneous crystallization	SHRIMP	Magyarosi and Rayner (2023)
21ZM081A01	12710	Deep Fox	Metaluminous granite	1269.0 ± 9.5 Ma	Igneous crystallization	SHRIMP	Magyarosi and Rayner (2023)
21ZM081A01	12710	Deep Fox	Metaluminous granite	1031 ± 15 Ma	Metamorphism	SHRIMP	Magyarosi and Rayner (2023)
21ZM176A01	12707	Deep Fox	Leucogabbro	*ca.* 1300 Ma	Igneous crystallization	SHRIMP	Magyarosi and Rayner (2023)
21ZM176A01	12707	Deep Fox	Leucogabbro	1038 ± 29 Ma	Metamorphism	SHRIMP	Magyarosi and Rayner (2023)
21ZM141A01	12708	HighREE	Granite	1648.7 ± 4.8	Igneous crystallization	SHRIMP	Magyarosi and Rayner (2024)
21ZM141A01	12708	HighREE	Granite	*ca.* 1005–950	Metamorphism/partial melting	SHRIMP	Magyarosi and Rayner (2024)
22ZM0427A01	12819	HighREE	Granite	1027.1 ± 8.2	Metamorphism/partial melting	SHRIMP	Magyarosi and Rayner (2024)
22ZM0427A01	12819	HighREE	Granite	986 ± 15	Metamorphism	SHRIMP	Magyarosi and Rayner (2024)
22ZM0370A01	12821	Oceanview	Syenite	1311 ± 12	Igneous crystallization	SHRIMP	Magyarosi and Rayner (2024)
22ZM0370A01	12821	Oceanview	Syenite	1018 ± 11	Metamorphism	SHRIMP	Magyarosi and Rayner (2024)
22ZM0337C01	12826	Pesky Hill	Pegmatite	*ca.* 1260	Igneous crystallization	SHRIMP	Magyarosi and Rayner (2024)
22ZM0337C01	12826	Pesky Hill	Pegmatite	1019.7 ± 8.2	Metamorphism	SHRIMP	Magyarosi and Rayner (2024)
22ZM0387A01	12820	Henley Harbour	Granite	1310 ± 12	Igneous crystallization	SHRIMP	Magyarosi and Rayner (2024)
22ZM0387A01	12820	Henley Harbour	Granite	1024.1 ± 8.2	Metamorphism/partial melting	SHRIMP	Magyarosi and Rayner (2024)
22ZM0349A01	12825	Long Point	Pegmatite	1500–2800 Ma	Inheritance	SHRIMP	Magyarosi and Rayner (2024)
22ZM0349A01	12825	Long Point	Pegmatite	1169 ± 11	Maximum age of crystallization	SHRIMP	Magyarosi and Rayner (2024)
22ZM0349A01	12825	Long Point	Pegmatite	1026 ± 11	Metamorphism	SHRIMP	Magyarosi and Rayner (2024)
FHWT-6-02		Foxtrot (SB)	Metaluminous rhyolite	1297 ± 21	Igneous crystallization	LA-ICPMS	Haley (2014)
FHWT-6-02		Foxtrot (SB)	Metaluminous rhyolite	1300 ± 2.5	Igneous crystallization	CA-TIMS	Haley (2014)
FH-10-02		Foxtrot	Pegmatite in basalt	1018 ± 30	Igneous crystallization	LA-ICPMS	Haley (2014)
FHC-44-01		Foxtrot (MTB)	Metaluminous rhyolite	1346 ± 51	Igneous crystallization	LA-ICPMS	Haley (2014)
FHC-45-01		Foxtrot (MTB)	Metaluminous rhyolite	1250 ± 20	Igneous crystallization	LA-ICPMS	Haley (2014)
FHC-33-01A		Foxtrot (RB)	Metaluminous rhyolite	1256 ± 24	Igneous crystallization	LA-ICPMS	Haley (2014)
FHC-33-01A		Foxtrot (RB)	Metaluminous rhyolite	1050 ± 21	Metamorphism	LA-ICPMS	Haley (2014)
FHC-34-03		Foxtrot (RB)	Metaluminous rhyolite	1047 ± 17	Metamorphism	LA-ICPMS	Haley (2014)

of a mantle enriched in volatiles and preferably REE and HFSE, commonly metasomatized by previous subduction (Beard *et al.*, 2022). They are located along deep-crustal structures that focus magma ascent from the mantle and occur in clusters, such as the one in the Gardar Province in Greenland. Despite the association of several critical minerals with alkaline igneous systems, genetic and exploration models are less developed than those for some of the other commodities such as gold, copper and iron.

REGIONAL GEOLOGY

The Grenville Province in eastern Labrador is composed of late Paleoproterozoic to Mesoproterozoic rocks (Figure 1) formed *via* multiple orogenic and related events including the Eagle River (1810–1775 Ma), Labradorian (1710–1600 Ma), Pinwarian (1520–1460 Ma) orogenies, Elsonian events (1460–1090 Ma), Grenvillian orogeny (1090–920 Ma) and Neoproterozoic and Phanerozoic events (Gower, 2019). It is subdivided into five terranes, namely, from north to south: the Groswater Bay, Hawke River (not shown on Figure 1), Lake Melville, Mealy Mountains and Pinware terranes (Figure 1; Gower, 2019). The terranes are distinguished from one another based on the type and degree of deformation and metamorphism they underwent during each orogenic event.

The occurrences are located in the Mealy Mountains and Pinware terranes. The Mealy Mountains terrane is composed of late Paleoproterozoic rocks consisting of gneisses, granitoids and other felsic rocks, and anorthositic, mafic and ultramafic rocks, and minor amounts of Mesoproterozoic rocks (Gower, 2019; van Nostrand, 1992; van Nostrand *et al.*, 1992; Nunn and van Nostrand, 1996a, b; Figure 1). Early Mesoproterozoic rocks (1600–1350 Ma) include the Pinware–Mealy Mountains terrane boundary comprising mafic and anorthositic rocks and anorthositic to felsic rocks of the Upper Paradise River Intrusive Suite. Middle Mesoproterozoic rocks (1350–1200 Ma) formed during the Elsonian events and include the REE-mineralized granitoids and syenite to monzonite and the Mealy diabase dykes. During the Grenville orogeny, the eastern Mealy Mountains terrane became structurally attenuated, reduced from approximately 80 km maximum width in the west, to approximately 5 km wide within the eastern structural wedge (Figure 1; Gower, 2019).

The Pinware terrane is mostly composed of foliated gneissic granitoids and minor mafic rocks varying in age from late Paleoproterozoic to late Mesoproterozoic and Neoproterozoic. Phanerozoic rocks occur in the southeast, along the shoreline, and consist of clastic sedimentary rocks and minor limestone.

LOCAL GEOLOGY

In the Mealy Mountains terrane, REE mineralization is hosted in granitoid and syenite to monzonite rocks occurring in an ~64-km long and up to 2-km wide mixed-class rock unit. It was formerly known as the Fox Harbour Volcanic Belt (Haley, 2014; Miller, 2015), but the volcanic origin of the rocks has been questioned and is currently under investigation. In this study, this mixed-class rock unit will be referred to as the Fox Harbour Belt (FHB) instead. The FHB consists of three sub-belts in the east and one sub-belt in the west, composed of quartz-saturated metaluminous to peralkaline and non-peralkaline granitoids, syenite, monzonite, mafic rocks, minor sedimentary rocks and quartzite (Haley, 2014; Miller, 2015; Magyarosi and Rayner, 2023). Based on the observed mineral assemblages and zircon growth at ~1.05 Ga, the rocks in FHB are interpreted to have experienced amphibolite-facies metamorphism during the Grenville orogeny (Haley, 2014). Deformation is more intense in the eastern part of the FHB, where the rocks are mylonitized. The main REE minerals are allanite, containing most of the LREE, and fergusonite, containing most of the HREE.

Rare-earth-element mineralization in the Pinware terrane is hosted in pegmatites classified as Group 2, formerly known as niobium–yttrium–fluorine (NYF) pegmatites (Wise *et al.*, 2022; Magyarosi and Rayner, 2024). These pegmatites are commonly associated with A-type peralkaline to metaluminous and mildly peraluminous parent intrusions and are typically hosted within or close to their parent intrusions, if there is one (Wise *et al.*, 2022). Previous geochronology and field relationships suggest that the pegmatites in the Pinware terrane are hosted in or closely associated with their parent intrusions ranging in composition from granite to syenite with less common granodiorite and syenodiorite (Magyarosi and Rayner, 2024). In this study, the pegmatites and their parent intrusions will be referred to as Fox Harbour South (FHS). The Pinware terrane in southeastern Labrador has been mapped at 1:100 000 scale (Gower, 2019); no detailed maps of the pegmatites and their parent intrusions exist and the extent of these intrusions is not known.

ANALYTICAL METHODS

The results of SHRIMP U–Pb analysis of seven samples (1 from Deep Fox, 3 from Fox Meadow, 2 from HighREE and 1 north of Foxtrot; Figure 1, Plate 1) were undertaken at the Geochronology Laboratories of the Geological Survey of Canada in Ottawa. The samples were disaggregated using standard crushing/pulverizing techniques followed by density separation using the Wilfley table and heavy liquids followed by magnetic separation. Grains selected for Sensitive High Resolution Ion Microprobe (SHRIMP) analysis were cast in epoxy mounts IP1061 and 1063. The mid-sections of

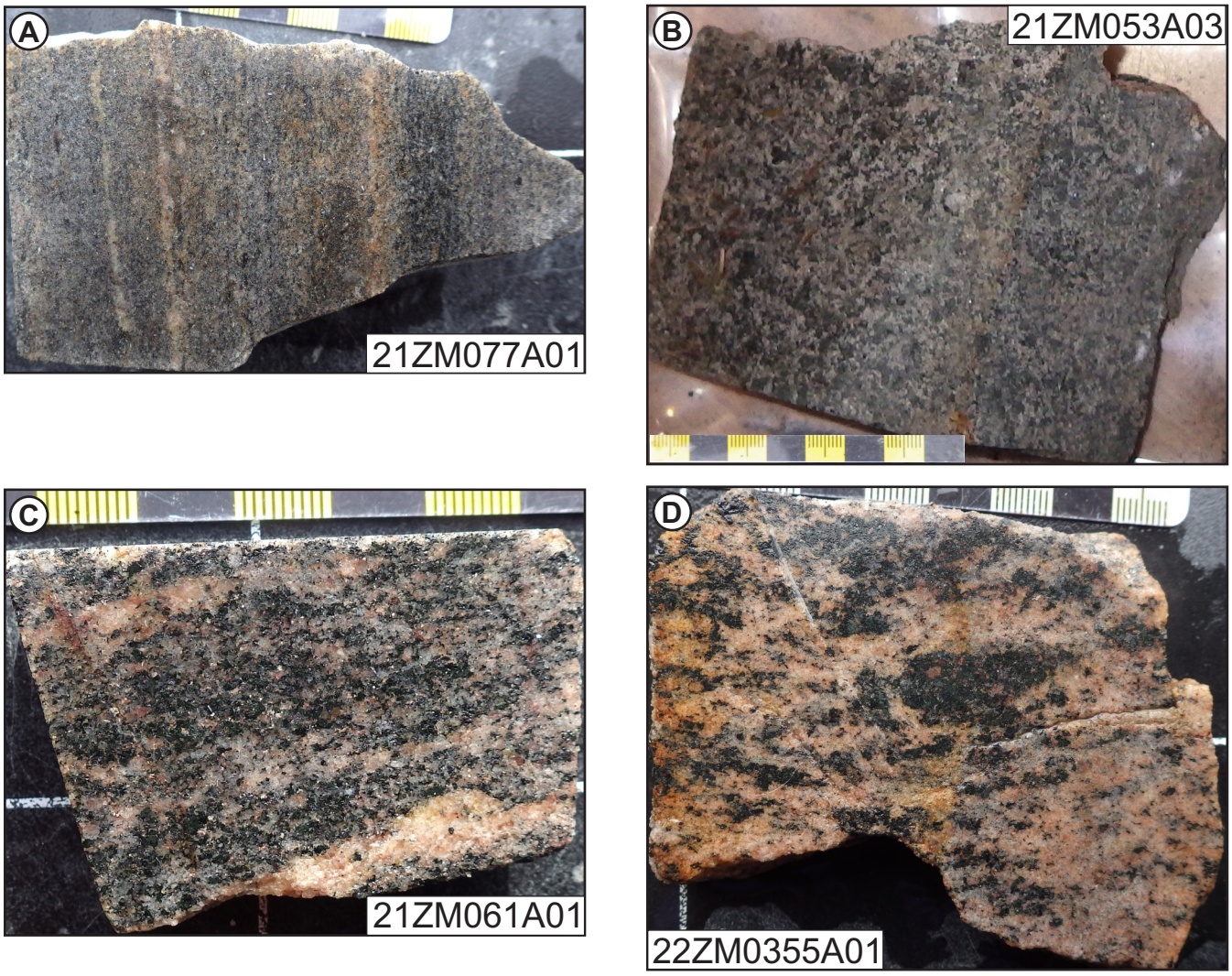

Plate 1. *Photos of slabs of samples used for geochronology analysis. A) Metaluminous granite from Deep Fox (21ZM077A01); B) Peralkaline monzonite from Fox Meadow (21ZM053A03); C) Peralkaline granodiorite from Fox Meadow (21ZM061A01); D) Peralkaline granite from Fox Meadow (22ZM0355A01).*

the minerals were exposed through polishing with diamond compound, and internal features characterized in cathodoluminescence (CL) and back-scattered electron (BSE) mode utilizing a Tescan Mira3 scanning electron microscope (SEM). Mount surfaces were evaporatively coated with 10 nm of high purity Au. SHRIMP analytical procedures followed those described by Stern (1997). Fragments of the Temora2 primary zircon reference material (RM) (GSC lab number 10493; $^{206}Pb/^{238}U$ age = 416.5 ± 0.22 Ma, Black *et al.*, 2004) and secondary zircon RMs 6266 ($^{206}Pb/^{238}U$ age = 559 ± 02 Ma, Stern and Amelin, 2003), 1242 ($^{207}Pb/^{206}Pb$ age = 2679.7 ± 0.2 Ma, Davis *et al.*, 2019) and 9910 (441.2 ± 0.4 Ma, B. Davis and V. McNicoll, unpublished data) were analyzed on the same mount and under the same conditions as the unknowns. Analyses were conducted using an O− primary beam, with a spot size of either 10 or 20 μm at a beam current between 3–8 nA. The count rates of the isotopes of U, Th and Pb as well as Hf and Yb for zircon were sequentially measured over six scans with a single electron multiplier. Offline data processing was accomplished using Squid3 (Bodorkos *et al.*, 2020) software. Decay constants follow the recommendations of Steiger and Jäger (1977). The 1σ error $^{206}Pb/^{238}U$ ratios reported in the Supplementary data table incorporate a ± 0.8% uncertainty in calibrating the primary RM (*see* Stern and Amelin, 2003). Analyses of a secondary zircon RM 1242 were interspersed between the sample analyses to assess the requirement of an isotopic mass fractionation correction for the $^{207}Pb/^{206}Pb$ age, however none was required. Details of the analytical session (mount/session number, spot size, primary beam intensity) are recorded in the footnotes of the data table as are the measured weighted mean age for the secondary RMs for that

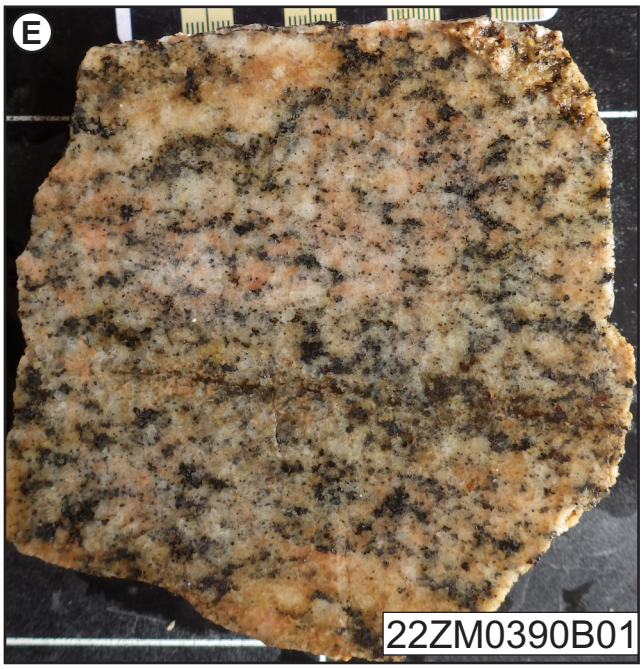

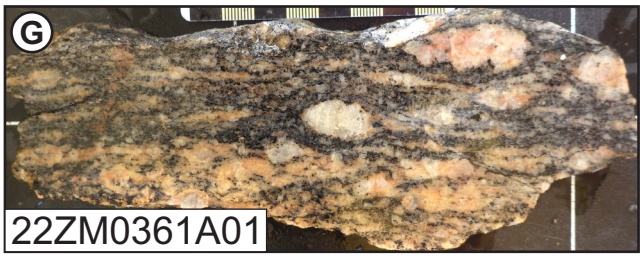

Plate 1 (Continued). *E) Metaluminous granite from HighREE (22ZM0390B01); F) Metaluminous granite from HighREE (22ZM0442A01); G) Augen gneiss north of Foxtrot (22ZM0361A01).*

session (Supplementary data). Common Pb correction utilized the surface Pb composition (Stern, 1997). Isoplot v. 4.15 (Ludwig, 2012) was used to generate concordia plots and calculate weighted means. The error ellipses on the concordia diagrams and the weighted mean errors are reported at 95% confidence, unless otherwise noted. An evaluation of the long-term reproducibility of $^{206}Pb/^{238}U$ age of secondary reference materials indicates that the minimum precision of SHRIMP ion probe weighted mean results is ± 0.78% (2σ, B. Davis pers. comm., 2023).

RESULTS

PETROGRAPHY

Sample 21ZM077A01 is a metaluminous granite from Deep Fox (1, Figure 1) composed of quartz, K-feldspar, albite, pyroxene, amphibole, biotite, magnetite, allanite, zircon and trace amounts of titanite, fluorite and apatite (Plate 1A). Pyroxene contains amphibole and biotite along cleavages, suggesting potassic alteration, with biotite also occurring as a primary mineral. Allanite is zoned and occurs as aggregates with zircon and locally apatite or disseminated or in pyroxene. Most of the zircon is small (<50 µm) and homogeneous, the larger grains (up to 200 µm) are zoned with a homogeneous rim and a cloudy core.

Sample 21ZM053A03 is a peralkaline monzonite from Fox Meadow (3, Figure 1) consisting of albite, K-feldspar, pyroxene, biotite, zircon, allanite and trace amounts of quartz, amphibole, magnetite, fergusonite and fluorite (Plate 1B). The amphibole is katophorite and less commonly riebeckite and the pyroxene is aegirine–augite. The amphibole typically occurs surrounding, and as oriented needles within, pyroxene, suggesting that it crystallized later. The biotite is annite and crystallized after amphibole and pyroxene. Biotite is very dark and contains zircon, allanite and fluorite, the last two along its cleavages. Allanite is also associated with zircon and fluorite, and locally forms late veins. Zircon mostly occurs as small (<50 µm) homogeneous grains (Plate 2A) or larger (up to 200 µm) grains with a cloudy, inclusion-rich core and homogeneous rim.

Sample 21ZM061A01 is a peralkaline granodiorite from Fox Meadow (3, Figure 1) composed of albite, quartz, K-feldspar, pyroxene, magnetite, biotite, zircon and REE

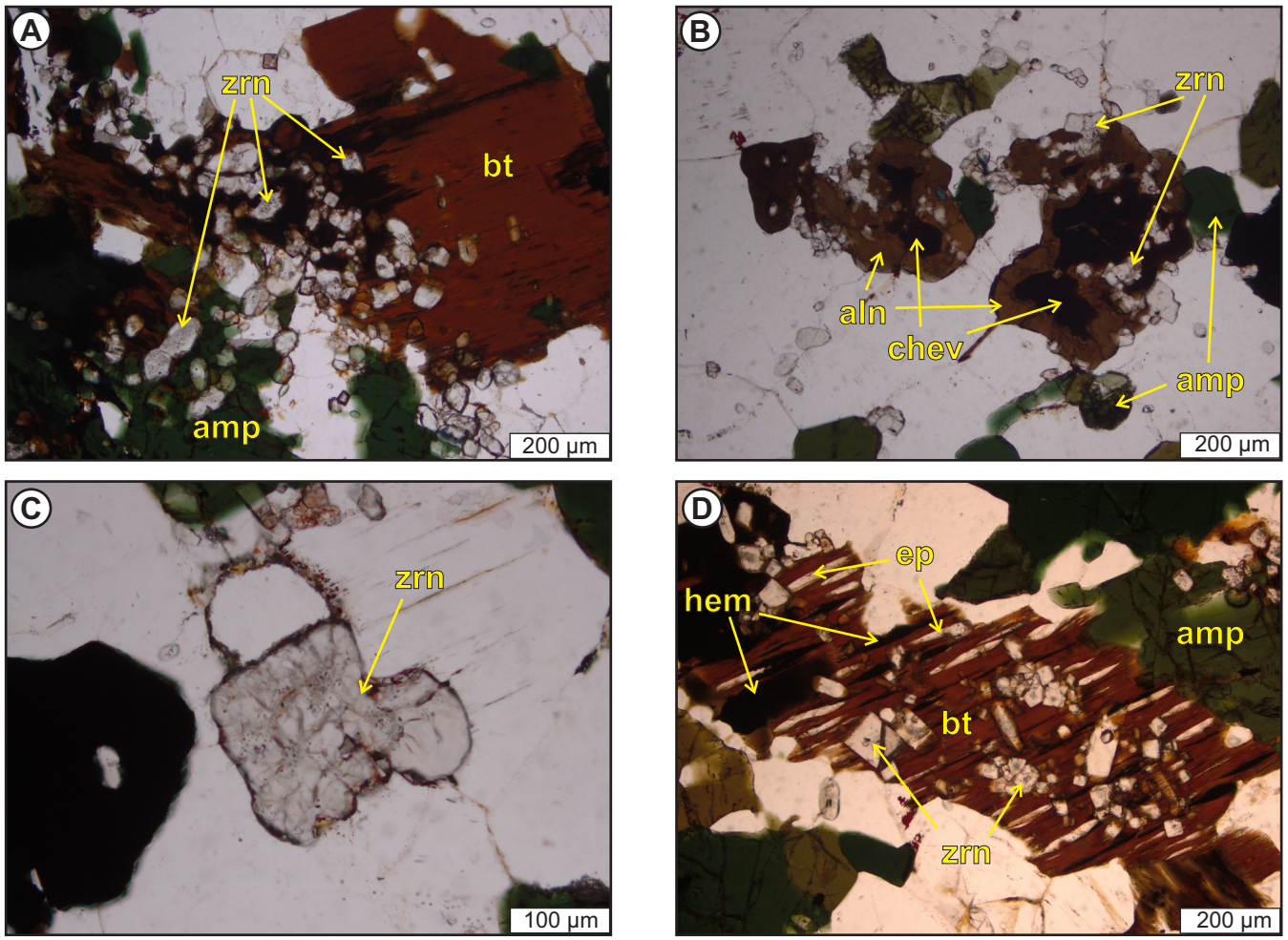

Plate 2. *Photomicrographs of samples used for geochronology analysis. A) Small zircon grains in biotite in sample 21ZM053A03; B) Zircon with allanite, chevkinite and amphibole in sample 21ZM061A01; C) Zoned zircon with inclusion-rich core and homogeneous rim in sample 21ZM061A01; D) Biotite containing inclusions of hematite, epidote and zircon in sample 22ZM0355A01.*

minerals (Plate 1C). Zircon ranges up to 200 µm, but generally less than 50 µm (Plate 2B). The larger ones are zoned with cloudy, inclusion-rich cores and homogenous rims (Plate 2C). The main REE minerals include chevkinite, which is typically surrounded by allanite (Plate 2B). Allanite also occurs as alteration in biotite and in a vein (~150 µm wide).

Sample 22ZM0355A01 is a peralkaline granite from Fox Meadow (3, Figure 1) consisting of K-feldspar, quartz, albite, pyroxene, amphibole, biotite, zircon, REE minerals, magnetite and trace amounts of ilmenite and hematite (Plate 1D). Amphibole occurs in pyroxene along cleavages or surrounding pyroxene. Biotite formed late, surrounding pyroxene and magnetite, and contains abundant zircon inclusions and hematite and epidote along cleavages (Plate 2D), suggesting that these minerals crystallized later. Magnetite contains ilmenite lamellae. Zircon grains are up to 200 µm, mostly homogeneous in composition but with some inclusion-rich cores (Plate 2D).

Sample 22ZM0390B01 is a metaluminous granite from the HighREE occurrence (4, Figure 1) composed of quartz, K-feldspar, albite, amphibole, magnetite, biotite, titanite, zircon, REE minerals, apatite and chlorite (Plate 1E). Magnetite is surrounded by titanite or biotite, which is mostly altered to chlorite. One large allanite grain (~1 mm) contains inclusions of ilmenite and titanite (Plate 2E), suggesting that allanite may have replaced primary chevkinite. Zircon occurs as grains up to 1 mm in length and contains abundant inclusions (Plate 2F).

Sample 22ZM0442A01 is a metaluminous granite from the HighREE occurrence (4, Figure 1) consisting of K-

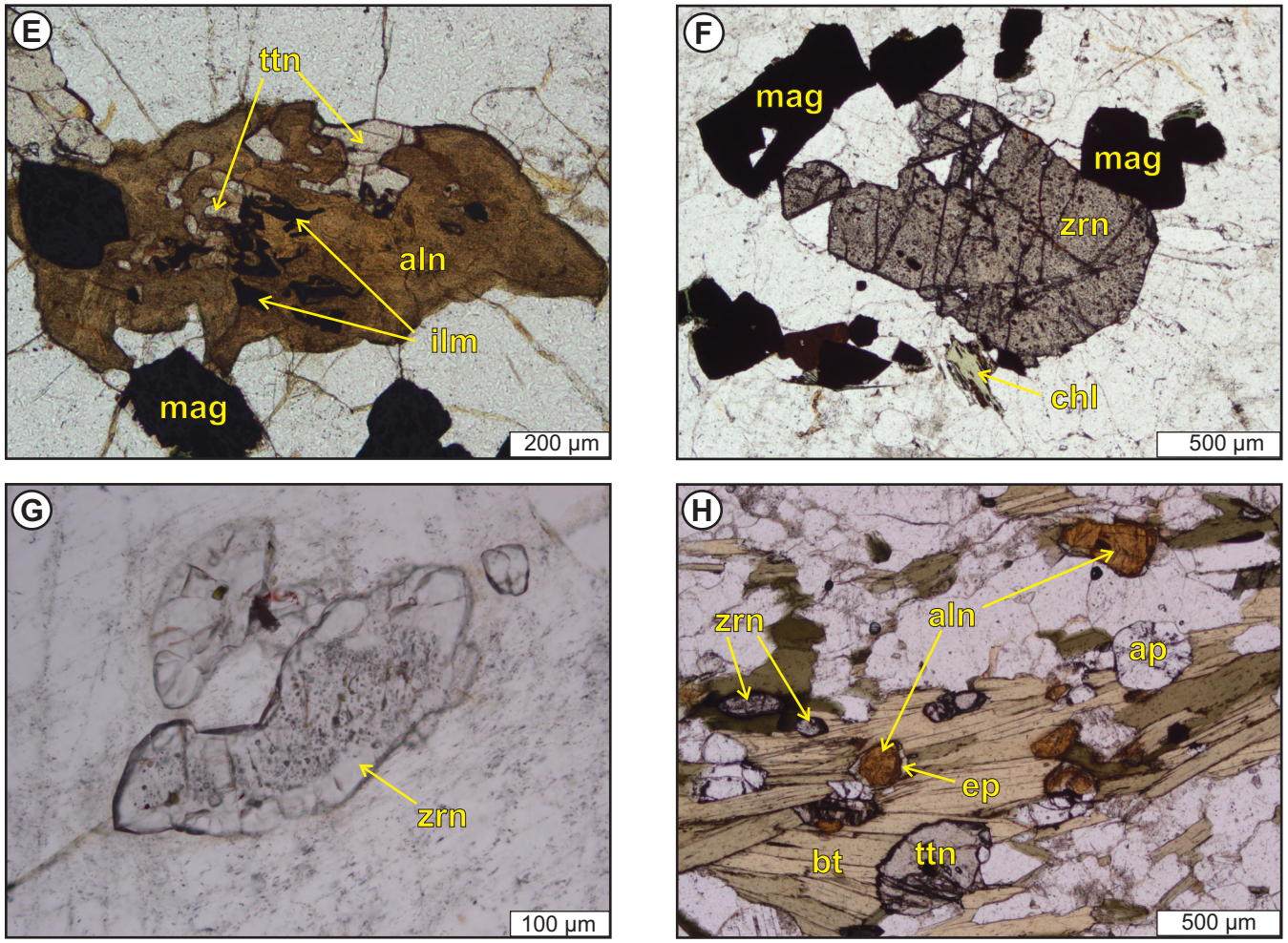

Plate 2 (Continued). *E) Allanite with inclusions of ilmenite and titanite in sample 22ZM0390B01; F) Inclusion-rich zircon in sample 22ZM0390B01; G) Zoned zircon with inclusion-rich core and homogeneous rim in sample 22ZM0442A01; H) Zircon in amphibole and biotite and allanite surrounded by epidote in biotite in sample 22ZM0361A01. Abbreviations on all plates are after Whitney and Evans (2010).*

feldspar, quartz, albite, amphibole, pyroxene, magnetite, zircon, allanite, apatite, ilmenite and hematite (Plate 1F). Quartz and K-feldspar locally form graphic texture. Pyroxene is light green (aegirine–augite), partially altered to chlorite and surrounded by amphibole, which is light to dark green, but less altered than pyroxene. Magnetite is surrounded by titanite and contains lamellae of ilmenite. Zircon is up to 500 µm and has inclusion-rich cores and homogeneous rims (Plate 2G). Allanite grains are up to 350 µm and are patchy.

Sample 22ZM0361A01 is an augen gneiss country-rock north of the Foxtrot occurrence (2, Figure 1), and is composed of quartz, K-feldspar, albite, biotite, titanite, allanite, magnetite, epidote, zircon, hematite and chlorite (Plate 1G). It contains local myrmekitic texture. Biotite is partially chloritized. Plagioclase is saussuritized. Allanite forms grains up to 100 µm surrounded by epidote (Plate 2H), but also occurs associated with titanite as small inclusions in titanite (<20 µm) or larger grains (<150 µm). Zircon is enclosed in biotite (Plate 2H).

GEOCHRONOLOGY

The geochronology results of the seven samples analyzed by SHRIMP are presented individually below with the interpretation of those results discussed in a combined section. They are also summarized in Figures 2 and 3 and Table 2.

21ZM077A01 Deep Fox Metaluminous Granite (GSC LAB # 12937)

Abundant clear colourless prismatic zircons were picked from the non-magnetic and magnetic fractions at 1° side slope of the Frantz separates sample. A large proportion of the grains exhibit cloudy cores in plane light. Cathodoluminescence images of the grains are characterized

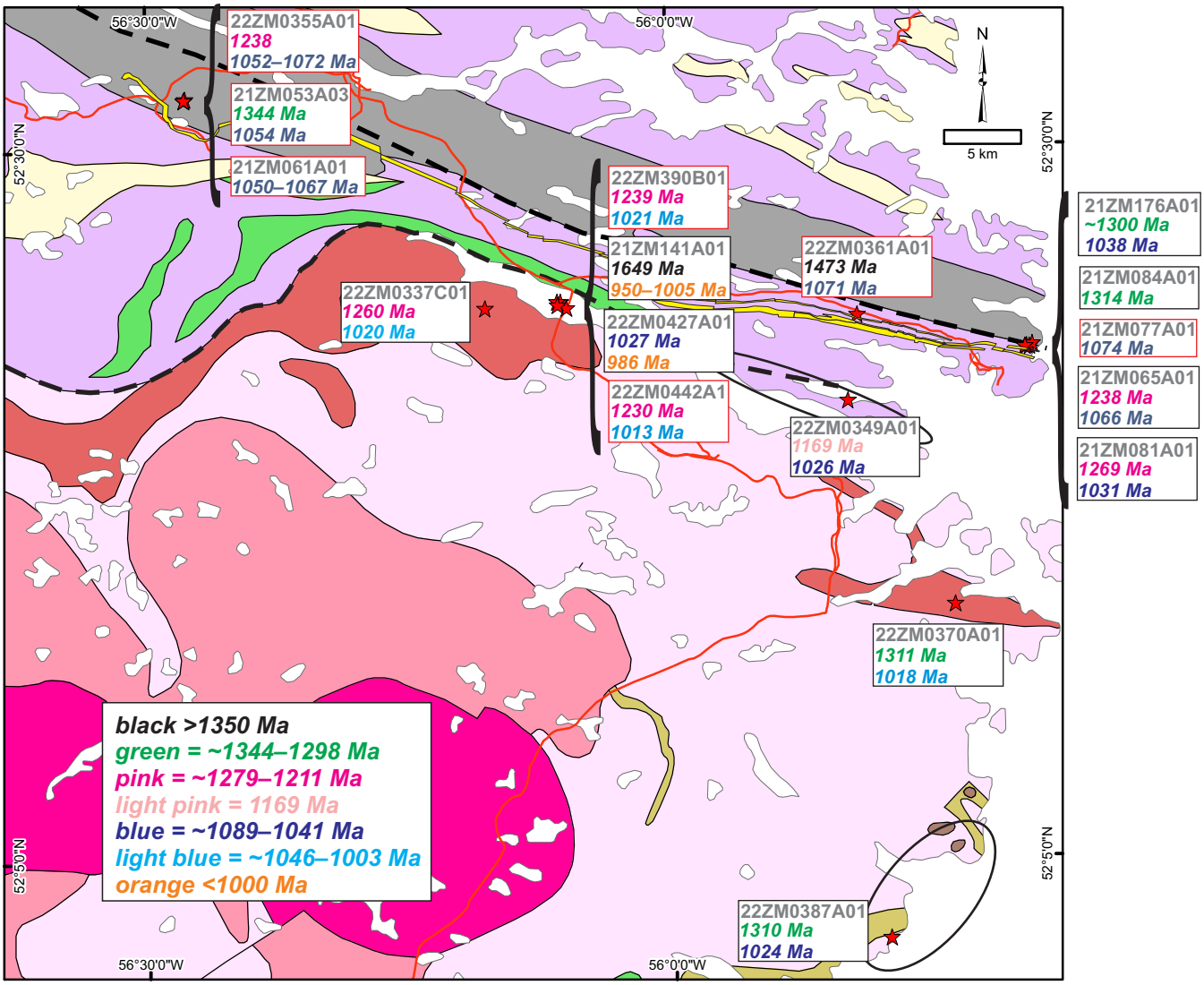

Figure 2. *Geochronology results from the FHB and FHS from this project (geology after Wardle* et al.*, 1997; Gower, 2010a, b, 2019). New data from this report are outlined in red rectangles. Ages are rounded and oldest core ages are also shown.* See *Figure 1 for legend.*

by regular sector zoned rims or entire grains (*e.g.*, grain 27, Figure 4A), as well as mosaic-textured outer parts of grains (*e.g.*, right side of grain 25, Figure 4A). The cloudy cores of these grains consist of abundant inclusions (*e.g.*, grain 24, 26, Figure 4A). Some of these inclusions are bright in BSE (not shown) and preliminary spot SEM-EDS analyses indicate that these are Y-REE silicates.

Thirty-three analyses were carried out on 33 grains. Regardless of subdividing the data by zoning style, the results overlap in age completely (Figure 4B). The mosaic cores and sector zoned rims range in age from 1058 to 1090 Ma. These form a single statistical population with a weighted mean $^{206}Pb/^{238}U$ age of 1074.4 ± 9.1 Ma (n=27, MSWD = 0.68, probability = 0.89) (Figure 4B). The inclusion-rich cores have single spot ages that range from 929 to 1098 Ma (red ellipses, Figure 4B) and, with the exception of one grain with extremely high common Pb content (14%, pink ellipse Figure 4B), all overlap in age with the mosaic and sector zoned zircon.

21ZM053A03 Fox Meadow Peralkaline Monzonite (GSC LAB # 12938)

Abundant zircons were recovered from this sample, those selected for geochronology were picked from the diamagnetic fraction and consist of clear colourless prismatic zircons. A large proportion of the grains exhibit a cloudy core in plane light. In CL images, the grains are characterized by regular sector zoned rims (*e.g.*, grains 93-95, Figure

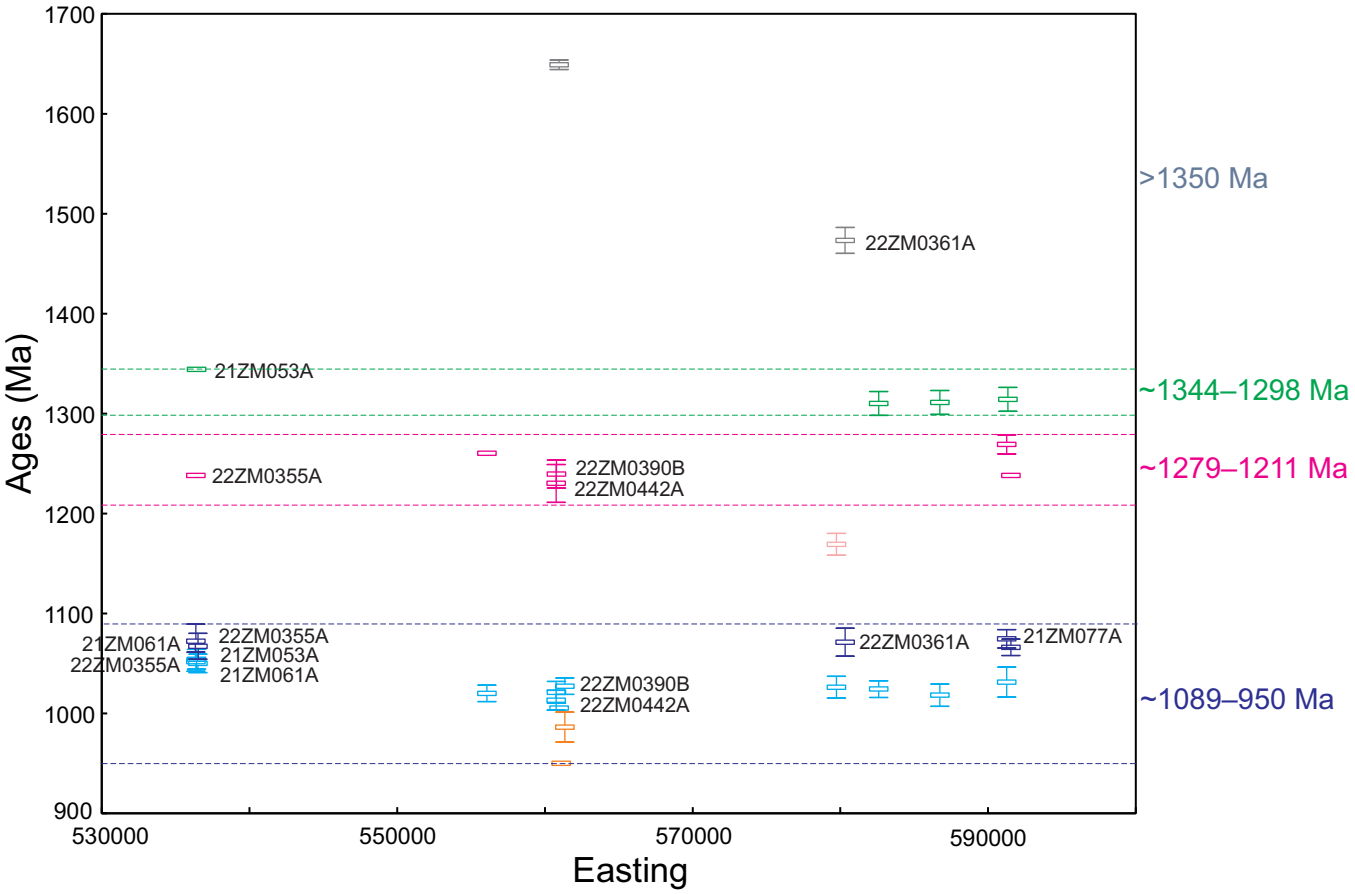

Figure 3. *Age* vs. *easting plot from the Fox Harbour Belt and Fox Harbour South. Only new data from this project are labelled. The last two digits of the sample numbers are omitted for brevity.*

Table 2. Summary of new SHRIMP U–Pb geochronology results

Sample number	Lab number	Area	Lithology	Age (Ma)	Interpretation
21ZM077A01	12937	Deep Fox	Metaluminous granite	1074.4 ± 9.1	Igneous crystallization/partial melting
21ZM053A03	12938	Fox Meadow	Peralkaline monzonite	1054.1 ± 9.9	Igneous crystallization/partial melting
21ZM061A01	12939	Fox Meadow	Peralkaline granodiorite	1049.8 ± 9.3	Igneous crystallization/partial melting
21ZM061A01	12939	Fox Meadow	Peralkaline granodiorite	1067 ± 13	Recrystallized core
22ZM0355A01	12824	Fox Meadow	Peralkaline granite	1051.5 ± 9.6	Igneous crystallization/partial melting
22ZM0355A01	12824	Fox Meadow	Peralkaline granite	1072 ± 17	Recrystallized core
22ZM0390B01	12941	HighREE	Metaluminous granite	1020.8 ± 11	Metamorphism/partial melting
22ZM0390B01	12941	HighREE	Metaluminous granite	1239 ± 14	Igneous crystallization
22ZM0442A01	12940	HighREE	Metaluminous granite	1013 ± 10	Metamorphism/partial melting
22ZM0442A01	12940	HighREE	Metaluminous granite	1230 ± 19	Igneous crystallization
22ZM0361A01	12823	North of Foxtrot	Augen gneiss	1071 ± 14	Metamorphism
22ZM0361A01	12823	North of Foxtrot	Augen gneiss	1473.0 ± 13	Igneous crystallization
22ZM0361A01	12823	North of Foxtrot	Augen gneiss	1705 ± 22	Inheritance (single analysis)

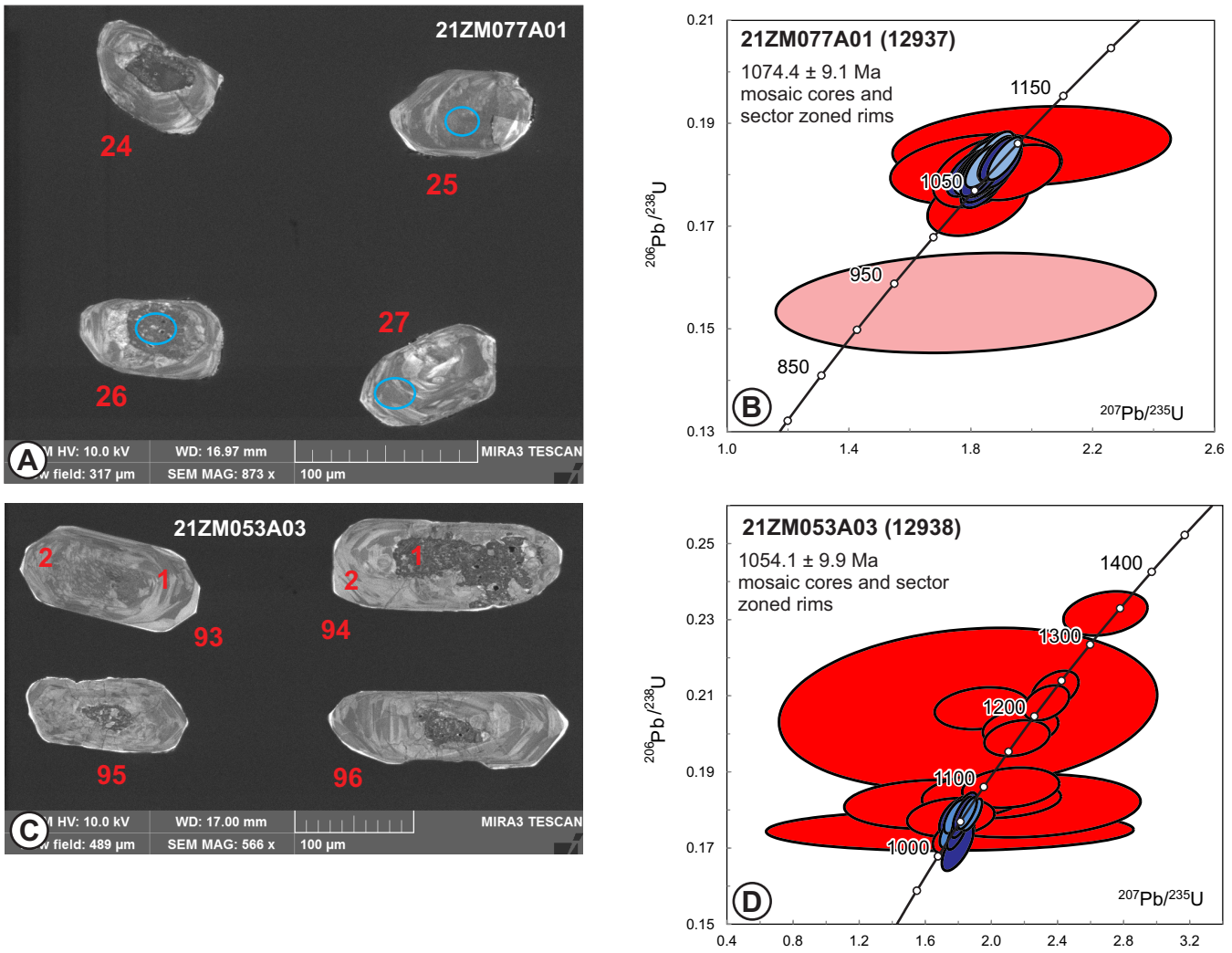

Figure 4. *Cathodoluminescence (CL) images and concordia diagrams for samples from Deep Fox and Fox Meadow field areas. Ellipses are plotted at the 95% confidence interval. In all sections, red ellipses represent analyses of inclusion-rich cores, light blue ellipses are from cores or inner parts of mosaic or sector zoned zircon, dark-blue ellipses represent analyses from rims or outer parts of mosaic or sector zoned zircon. Pink ellipses are anomalous inclusion-rich zircon. Ages given on the concordia diagrams are weighted mean $^{206}Pb/^{238}U$ ages along with their external uncertainty.* See *text for discussion.*

4C) or entire grains and cores that are either mosaic-textured/mottled (*e.g.*, grain 93, Figure 4C) or contain abundant inclusions (*e.g.*, grains 94 and 96, Figure 4C).

Thirty-one analyses were carried out on 24 grains. The data can be subdivided by zoning style into two age groups – the inclusion-rich cores are characterized by a wide spread of ages from 1026 to 1344 Ma (red ellipses, Figure 4D). These are loosely clustered at *ca.* 1.05 and 1.2 Ga. The mosaic cores and sector zoned rims form a single statistical population with a weighted mean $^{206}Pb/^{238}U$ age of 1054.1 ± 9.9 Ma (n=13, MSWD = 1.12, probability = 0.33) (blue ellipses, Figure 4D). In some cases, the mosaic texture appears to grade into the more organized sector zoning (*e.g.*, grain 93, Figure 4C), consistent with their coeval results.

21ZM061A01 Fox Meadow Peralkaline Granodiorite (GSC LAB # 12939)

Abundant zircons were recovered from this sample, those selected for geochronology were picked from the diamagnetic fraction. In plane light these appear as clear, colourless, prismatic zircon grains with a large proportion exhibiting cloudy cores as seen in the other samples described herein. Similar to 12937 and 12938, CL images are characterized by regular sector-zoned grains (*e.g.*, grain 22, Figure 4E) or rims (*e.g.*, grain 21, Figure 4E), or mosaic-textured outer parts of grains (*e.g.*, right side of grain 23, Figure 4E). The cloudy cores of these grains consist of abundant inclusions (*e.g.*, grains 21, 23 and 24, Figure 4E); some of which are bright in BSE.

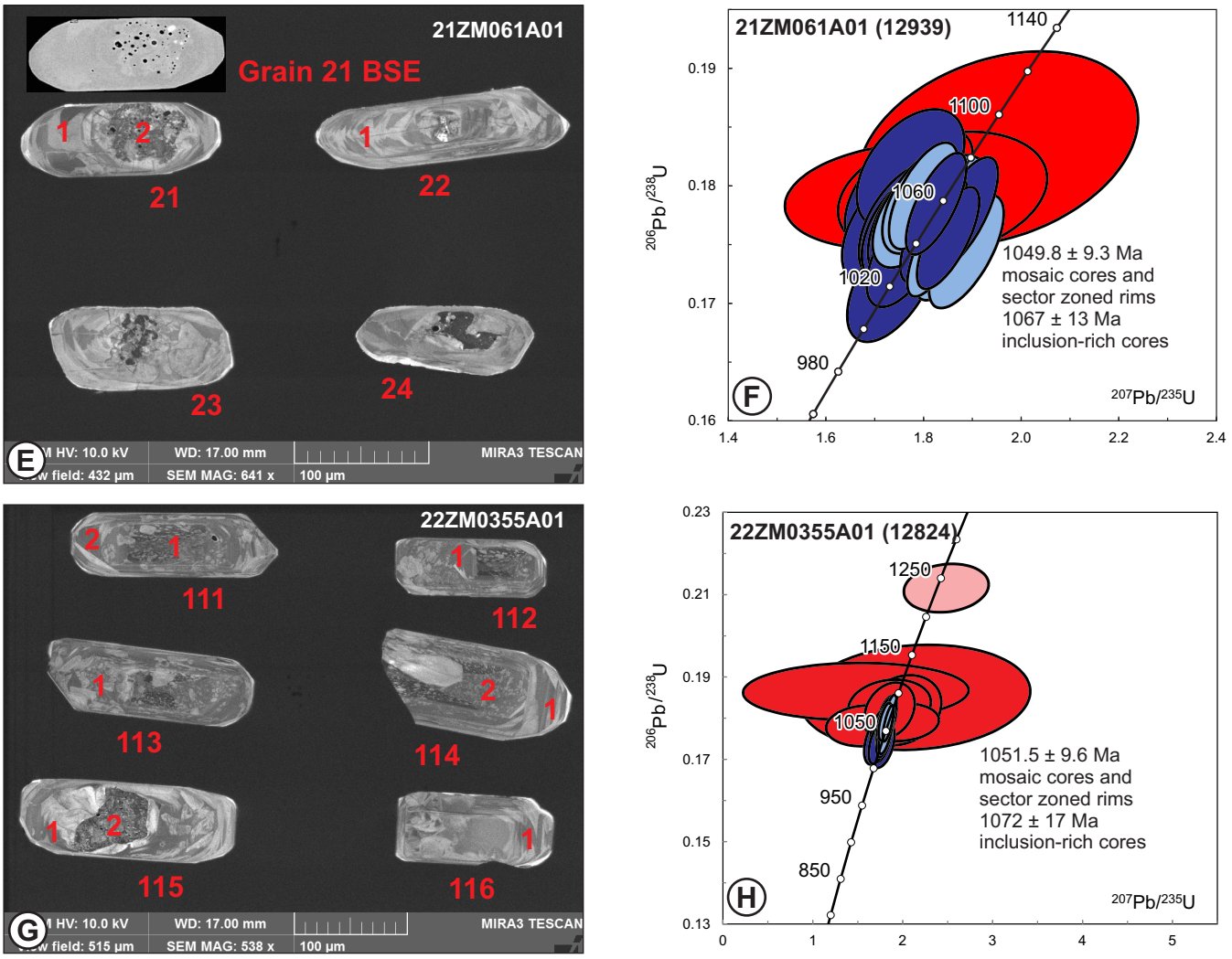

Figure 4 (Continued).

Twenty-nine analyses were carried out on 23 grains. If subdivided by zoning style, the individual grain dates all overlap one another (Figure 4F). The mosaic cores and sector zoned rims range in age from 1022 to 1075 Ma (light and dark blue ellipses, Figure 4F) and form a single statistical population with a weighted mean $^{206}Pb/^{238}U$ age of 1049.8 ± 9.3 Ma (n=23, MSWD = 1.00, probability = 0.46). The inclusion-rich cores range in age from 1059 to 1084 Ma (red ellipses, Figure 4F), with a weighted mean $^{206}Pb/^{238}U$ age of 1067 ± 13 Ma (n=6, MSWD = 0.31, probability = 0.91). While this mean age is slightly older than the rims as would be expected, there is still overlap within measured uncertainties.

22ZM0355A01 Fox Meadow Peralkaline Granite (GSC LAB # 12824)

The abundant zircon recovered from this sample are identical in appearance to the other three samples described above. They are clear, colourless and prismatic and possess distinct cloudy cores. In CL images, they exhibit the same inclusion-rich or mosaic textured cores (*e.g.*, grains 111–115, Figure 4G) and sector zoned rims (*e.g.*, grains 111–115, Figure 4G) or entire grains (*e.g.*, 116, Figure 4G). Some of the inclusions are bright in BSE.

Twenty-nine analyses were carried out on 20 zircon grains. The mosaic cores and sector zoned rims and grains range in age from 1032 to 1072 Ma and form a single statistical population with a weighted mean $^{206}Pb/^{238}U$ age of 1051.5 ± 9.6 Ma (n=20, MSWD = 1.05, probability = 0.40) (light and dark blue ellipses, Figure 4H). The inclusion-rich cores range in age from 1013 to 1238 Ma. Excluding the oldest core analysis (pink ellipse, Figure 4H), these cores yield a weighted mean $^{206}Pb/^{238}U$ age of 1072 ± 17 Ma (n=8, MSWD = 1.3, probability = 0.22) (red ellipses, Figure 4H), which is indistinguishable from the rim data within uncertainty. A second analysis was carried out in the core to try to reproduce the older age. This second analysis falls within

the 1072 Ma group but suggests that the inclusion-rich core may be fully- or nearly fully recrystallized zircon from older, precursor material.

INTERPRETATION OF DEEP FOX AND FOX MEADOW RESULTS

The appearance of the zircons and their geochronology results are consistent across the 3 samples from Fox Meadow to the one sample from Deep Fox. They are dominated by sector zoned zircon (both as rims and cores), with unusual mosaic textured cores. These two zoning types can be combined within each sample to yield mean ages of 1074.4 ± 9.1 Ma (sample 21ZM077A01), 1054.1 ± 9.9 Ma (sample 21ZM053A03), 1049.8 ± 9.3 Ma (sample 21ZM061A01) and 1051.5 ± 9.6 Ma (sample 22ZM0355A01). Sector zoning in zircon is generally taken to indicate growth from a magma (Corfu *et al.*, 2003), hence these ages are interpreted as igneous crystallization ages. All of these samples contain abundant zircon and the clear, colourless sector zoned zircon dominates the population volumetrically as well. The inclusion-rich zircons return similar ages to the sector zoned zircon but tend to skew to older ages, with the oldest single ages at 1098 ± 34 Ma (sample 21ZM077A01), 1344 ± 24 Ma (sample 21ZM053A01), 1084 ± 36 Ma (sample 21ZM061A01) and 1238 ± 13 Ma (sample 22ZM0355A01). One interpretation of the data is that a *ca.* 1.05–1.07 Ga event resulted in the profound recrystallization of the original igneous zircon. In some samples (21ZM077A01 and 21ZM061A01) of the inclusion-rich cores, recrystallization was essentially complete as there is no statistically significant distinction in age. Likewise, the mosaic textured zircon cores may represent a fully recrystallized core where all record of an older U–Pb signature has been lost. In other samples, the oldest single analysis from an inclusion-rich core may represent the minimum original protolith crystallization age: 1344 ± 24 Ma and 1238 ± 13 Ma from samples 21ZM053A01 and 22ZM0355A01, respectively. Similar zircon recrystallization was described by Kärenlampi *et al.* (2020) in a Paleoproterozoic Nb–Zr–REE-mineralized A1-type intrusion in Finland, where the igneous zircon cores were variably recrystallized during subsequent metamorphism, resulting in scatter of the U–Pb age data.

22ZM0390B01 HighREE Metaluminous Granite (GSC LAB # 12941)

The zircon grains recovered from this sample are abundant, clear, colourless, prismatic to ovoid. In plane light, cores are visible, some of which are inclusion-rich while others are defined primarily by fractures that radiate from them. In CL imagery, sector zoning is dominant (*e.g.*, grains 71–74, Figure 5A), however some grains appear to contain both sector zoned cores and rims (*e.g.*, grains 72 and 73, Figure 5A). The cloudy, inclusion-rich cores appear dark in CL (*e.g.*, grain 74, Figure 5A).

Thirty-seven analyses were carried out on 29 separate zircon grains (Figure 5B). The oldest cluster of six analyses comes from sector-zoned zircon cores that are characterized by fine-scale zoning within each sector (green ellipses, Figure 5B). These yield a weighted mean $^{206}Pb/^{238}U$ age of 1239 ± 14 Ma (n=6, MSWD = 0.90, probability = 0.48). Sector zoned zircon rims yield a weighted mean $^{206}Pb/^{238}U$ age of 1021 ± 11 Ma (n=11, MSWD = 1.5, probability = 0.12, dark blue ellipses, Figure 5B). There are other analyses of sector zoned zircon that fall between these two ages that are inferred to be mixed analytical spots as the two types of sector zoned zircon are difficult to distinguish from one another. Analytical spots on inclusion-rich zircon cores return ages spanning nearly the entire range of the other two distinct groups, from 1005 to 1204 Ma (red ellipses, Figure 5B).

22ZM0442A01 HighREE Metaluminous Granite (GSC LAB # 12940)

The zircons recovered from this second HighREE sample are very similar to the other HighREE sample described immediately above. They are prismatic to ovoid, sharply terminated, clear and colourless with both clear and cloudy cores visible in plane light. In CL, sector zoning dominates the rims (*e.g.*, grains 103–106, Figure 5C), and is also observed in some cores (*e.g.*, grain 105, Figure 5C). Inclusion-rich cores are generally dark in CL (*e.g.*, grain 104, Figure 5C).

Thirty analyses were carried out on 20 separate zircon grains and the results are virtually identical to the sample described previously (GSC Lab # 12941). The oldest cluster of six analyses comes from sector-zoned zircon cores that are characterized by fine scale zoning within each sector (green ellipses, Figure 5D). These yield a weighted mean $^{206}Pb/^{238}U$ age of 1230 ± 19 Ma (n=6, MSWD = 1.3, probability = 0.28). Sector zoned zircon rim data yields a weighted mean $^{206}Pb/^{238}U$ age of 1013 ± 10 Ma (n=8, MSWD = 1.2, probability = 0.30, blue ellipses, Figure 5D). Only one slightly young analysis was excluded from the older group (light green ellipse, Figure 5D) and may be the result of mixing with an undetected young sector-zoned rim. Analytical spots on inclusion-rich zircon return relatively imprecise dates that scatter around the younger age group ranging from 934 to 1108 Ma (red ellipses, Figure 5D).

22ZM0361A01 North Foxtrot Augen Gneiss Country Rock (GSC LAB # 12823)

Pale-brown prismatic zircons with extensive inclusions and moderate fracturing were picked from the diamagnetic

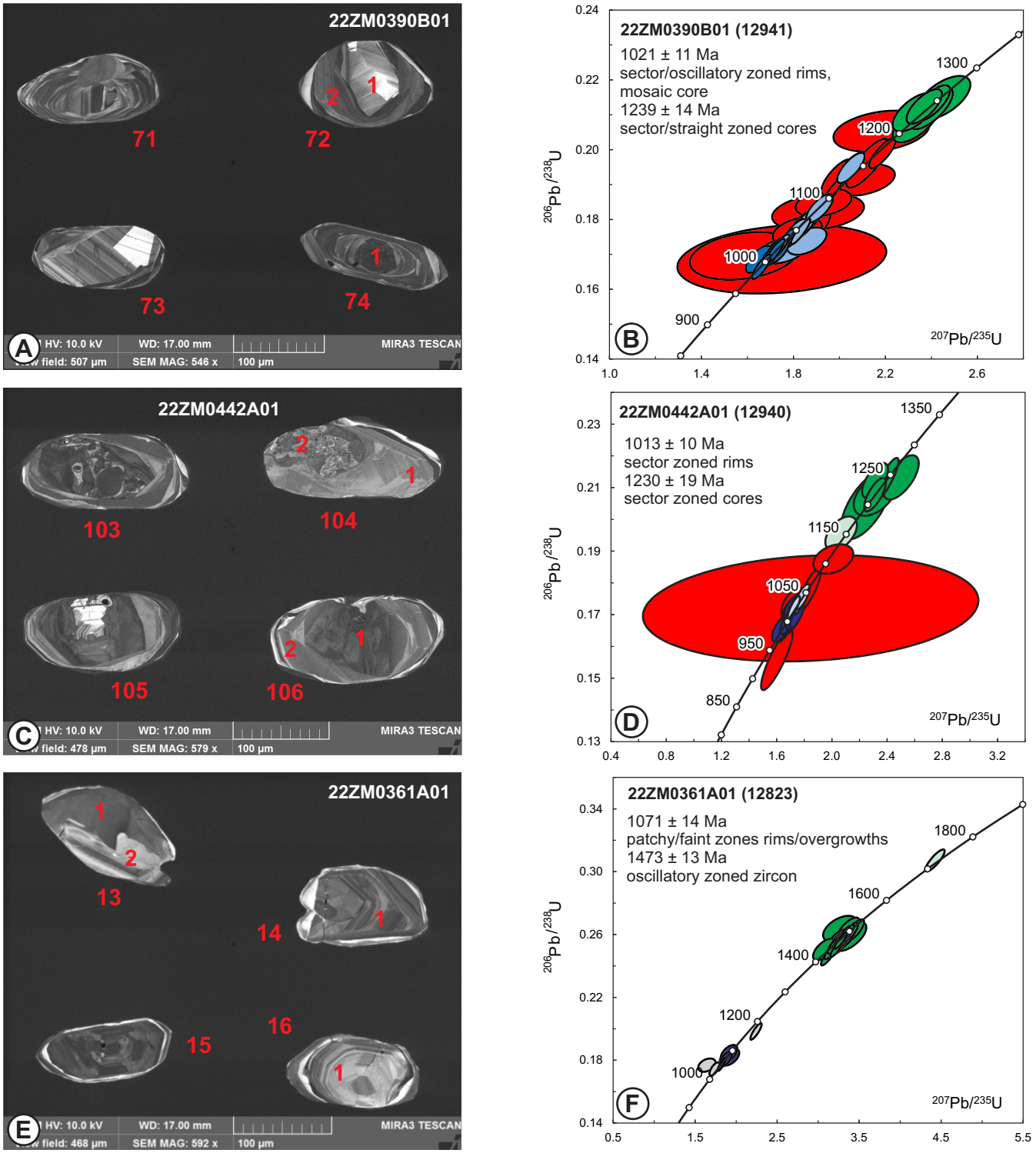

Figure 5. *Cathodoluminescence (CL) images and concordia diagrams for plutonic rocks from HighREE and country rock from north of the Foxtrot occurrence. Ellipses are plotted at the 95% confidence interval. In all sections of the figure, green ellipses represent analyses of sector/oscillatory zoned cores interpreted as representing igneous zircon and red ellipses represent inclusion-rich zircon. Light-blue ellipses are from sector/mosaic zoned zircon cores or inner parts of grains, while dark blue ellipses represent analyses from sector zoned rims. Light-green or grey ellipses represent anomalous analyses. Ages given on the concordia diagrams are weighted mean $^{206}Pb/^{238}U$ ages along with their external uncertainty.* See *text for discussion.*

to magnetic fraction at 3° side slope Frantz separates. In contrast to the other samples in this report, the inclusions are dispersed throughout the grain, not concentrated in a cloudy core. In CL images, these grains are typically oscillatory ± sector zoned (*e.g.*, grains 14–16, Figure 5E). Patchy rims or overgrowths are common, but these are often less than 10 µm across (*e.g.*, grain 13–16, the overgrowth on grain 13 is large enough to permit analysis, Figure 5E).

Forty analyses were carried out on 32 individual zircon grains that cluster in two main groups. The oscillatory zoned zircon (green ellipses, Figure 5F) data forms a well-defined cluster (Figure 5F) with a weighted mean $^{206}Pb/^{238}U$ age of 1473 ± 13 Ma (n=31, MSWD = 1.6, probability = 0.02). This excludes one distinctly older grain (*ca.* 1.7 Ga, light green ellipse, Figure 5F) as well as one slightly younger grain excluded on a statistical basis. The dates of the zircon rims/overgrowths range from 1037 to 1167 Ma (dark blue/grey ellipses, Figure 5F). The oldest rim analysis (grey ellipse, Figure 5F) is discordant and is inferred to be due to analytical spot overlap with the older 1473 Ma material. A cluster of the most concordant rim analyses return a weighted mean $^{206}Pb/^{238}U$ age of 1071 ± 14 Ma (n=4, MSWD = 2.2, probability = 0.09). Two slightly younger and reversely discordant analyses were excluded from the calculation of this mean (grey ellipses, Figure 5F).

INTERPRETATION OF HIGHREE AND NORTH FOXTROT RESULTS

While similar in appearance to the zircons from igneous precursor rocks at Deep Fox and Fox Meadow with their cloudy inclusion-rich cores and sector zoned rims, the rocks at HighREE preserve sector and finely zoned zircon in their cores with distinct and reproducible ages relative to their rims. These older core ages of 1239 ± 14 Ma and 1230 ± 19 Ma for samples 22ZM0390B01 and 22ZM0442A01, respectively, are interpreted as the igneous crystallization ages of the metaluminous granites. The sector zoned rims with ages of 1021 ± 11 Ma and 1013 ± 10 Ma (samples 22ZM0390B01 and 22ZM0442A01, respectively) are interpreted to represent a metamorphic event, although as discussed above, given the sector zoning in these rims, which is generally indicative of growth in a fluid/magmatic environment, these may represent an episode of partial melting. Both igneous crystallization and metamorphism/ partial melting in each of the two HighREE metaluminous granites are coeval with one another.

The 1473 ± 13 Ma age from augen gneiss north of Foxtrot is interpreted as the crystallization age. The less well-constrained age of 1071 ± 14 Ma from zircon rims is interpreted as the metamorphic age. This age of metamorphism is also known at Deep Fox (1065.9 ± 8.2 Ma, Magyarosi and Rayner, 2023) as well as Fox Meadow.

DISCUSSION

Previous analyses of the Fox Harbour alkaline-silicate rocks returned two clusters of igneous ages separated by ~60 Ma, one between *ca.* 1344 and 1298 Ma and the other between *ca.* 1279 and 1211 Ma, with the older age being more common in the east and the younger age being more common in the west (Table 1, Figures 2 and 3), although this may be due to the lack of additional geochronology data. Dated samples in this report from Deep Fox and Fox Meadow are similar to the rest of FHB, supporting the interpretation of two igneous stages, one *ca.* 1.24 and the other *ca.* 1.34 Ga, based on the oldest single ages preserved in the inclusion-rich cores. In this study, one of the older ages was determined from a sample in the west (sample 21ZM053A01, 1344 ± 24 Ma), suggesting that the older age may be more widespread, at least along the FHB. Grenville-age zircon in the FHB (ranging between 1049.8 ± 9.3 and 1074.4 ± 9.1 Ma), occurring both as new growth (sector zoned) and recrystallized material (mosaic texture) dominate the zircon population. Profound partial melting, or addition of silicate melts, would be required for the extensive growth of the 1.05–1.07 Ga sector-zoned zircon observed here.

Igneous crystallization ages of *ca.* 1230–1239 Ma at HighREE indicate that these granites are part of FHS, as previously suggested (Magyarosi and Rayner, 2024), and further indicates that they represent the parent intrusions of the REE pegmatites based on spatial association. Although, pegmatites from HighREE were not dated, the similar age of a REE-rich pegmatite from the nearby Pesky Hill (Table 1) also points to the strong genetic link between pegmatites and spatially associated intrusions. The older igneous age of *ca.* 1310 Ma was not detected in the HighREE samples.

Metamorphism resulted in various degrees of recrystallization of the inclusion-rich zircon cores, as discussed earlier, and rim overgrowths are observed in most samples. The metamorphic ages in the analyzed samples show two clusters: one between *ca.* 1050 and 1075 Ma, present in the FHB samples and its host rock north of Foxtrot, and the other between *ca.* 1013 and 1021 Ma in the HighREE samples. These results are consistent with previous results (*see* Table 1, Figures 2 and 3).

The augen gneiss, located north of the Foxtrot occurrence, yields a crystallization age of 1473 ± 13 Ma along with inheritance at *ca.* 1700 Ma, which is consistent with ages of the rocks from the surrounding area although it is more com-

mon in the Pinware terrane (Tucker and Gower, 1994; Haley, 2014; Prieto Moreno, pers. comm., 2024). This result resolves the controversy regarding the spatial extent of the FHB (Magyarosi, 2022). It confirms that the FHB intrudes older rocks, which are not part of the alkaline-silicate igneous system (Miller, 2015; Gower, 2019). However, the reason for the more widespread presence of this Pinwarian age in the Mealy Mountains terrane will need more detailed work from a tectonic and structural perspective.

ACKNOWLEDGMENTS

This paper is a contribution to Natural Resources Canada's (NRCan) TGI Program of the GSC. Support for this study was provided through the Magmatic Ore Systems 'Sub-Activity (Critical minerals within carbonatite, syenite and allied peralkaline–alkaline rocks in the central and eastern parts of the Canadian Shield: Where, when, how, were they formed') and by the GSNL. ZM is grateful for the support provided by Search Minerals Inc., especially Randy Miller, throughout the whole project. Lindsay Oldham and Arianna Sheppard are thanked for their assistance in the field in the summers of 2021 and 2022. Cartographic support was provided by Kim Morgan and Peter Bruce, GSNL. John Hinchey, GSNL, is thanked for his support in every aspect of the work. Anne-Aurélie Sappin from the GSC and Dave Corrigan, formerly from the GSC, are thanked for their liaison with the GSC. Dylan Goudie and Wanda Aylward provided assistance with the SEM/SEM-MLA and EPMA analyses at MUN, respectively. NR is grateful for the support and assistance of the staff of the Geochronology Laboratories of the Geological Survey of Canada. In particular, Ray Chung, Greg Case and Tom Pestaj are thanked for their careful efforts and excellent work. Matt Polivchuk provided the necessary high-quality scanning electron microscope images. Discussions with Dr. Eric Thiessen and Nicolas Prieto Moreno about the geology of the study area were greatly appreciated by ZM.

REFERENCES

Beard, C.D., Goodenough, K.M., Borst, A.M., Wall, F., Siegfried, P.R., Deady, E.A., Pohl, C., Hutchison, W., Finch, A.A., Walter, B.F., Elliott, H.A.L. and Brauch, K.
2022: Alkaline-silicate REE-HFSE systems. Economic Geology Volume 118, pages 177-208. https://doi.org/10.5382/econgeo.4956.

Black, L.P., Kamo, S.L., Allen, C.M., Davis, D.W., Aleinikoff, J.N., Valley, J.W., Mundil, R., Campbell, I.H., Korsh, R.J., Williams, I.S. and Foudoulis, C.
2004: Improved $^{206}Pb/^{238}U$ microprobe geochronology by monitoring of a trace-element-related matrix effect; SHRIMP, ID-TIMS, ELA-ICP-MS and oxygen isotope documentation for a series of zircon standards. Chemical Geology, Volume 205, pages 115-140.

Bodorkos, S., Bowring, J. and Rayner, N.
2020: Squid3: Next-generation data processing software for Sensitive High Resolution Ion Micro Probe (SHRIMP). Exploring for the Future: Abstracts. Geoscience Australia. https://doi.org/10.11636/133870.

Corfu, F., Hanchar, J.M., Hoskin, P.W.O. and Kinny, P.
2003: Atlas of zircon textures. Reviews in Mineralogy and Geochemistry, Volume 53, pages 469-500. https://doi.org/10.2113/0530469

Crocker, M.G.
2014: A petrographic, geochemical and geochronological study of rare earth mineralization in the Red Wine Intrusive Suite, Labrador, Canada. Unpublished M.Sc. thesis. Memorial University of Newfoundland, St. John's, Newfoundland,766 pages.

Davis, W.J., Pestaj, T., Rayner, N. and McNicoll, V.M.
2019: Long-term reproducibility of $^{207}Pb/^{206}Pb$ age at the GSC SHRIMP lab based on the GSC Archean reference zircon z1242. Geological Survey of Canada, Scientific Presentation 111, 1 poster. https://doi.org/10.4095/321203

Ducharme, T.A., McFarlane, C.R.M., van Rooyen, D. and Corrigan, D.
2021: Petrogenesis of the peralkaline Flowers River Igneous Suite and its significance to the development of the southern Nain Batholith. Geological Magazine, Volume 168, pages 1911-1936.

Gower, C.F.
2010a: Bedrock geological maps for the Grenville Province and adjacent Makkovik in eastern Labrador. Government of Newfoundland and Labrador, Department of Natural Resources, Geological Survey, Maps 2010-01 to 2010-25, 1:100 000 scale.

2010b: Geology of the Grenville Province and adjacent eastern Makkovik Province, eastern Labrador. Government of Newfoundland and Labrador, Department of Natural Resources, Geological Survey, Map 2010-50, scale 1:500 000.

2019: Regional geology of eastern Labrador (eastern Makkovik and Grenville provinces). Government of Newfoundland and Labrador, Department of Natural Resources, Geological Survey, Memoir 4, 654 pages.

Haley, J.T.
2014: 1.3 Ga bimodal volcanism in southeastern Labrador: Fox Harbour. Unpublished M.Sc. thesis. Memorial University of Newfoundland, St. John's, Newfoundland, 209 pages.

Horstwood, M.S.A., Košler, J., Gehrels, G., Jackson, S.E., McLean, N.M., Paton, C., Pearson, N.J., Sircombe, K., Sylvester, P., Vermeesch, P., Bowring, J.F., Condon, D.J. and Schoene, B.
2016: Community-derived standards for LA-ICP-MS U-(Th-)Pb geochronology – uncertainty propagation, age interpretation and data reporting. Geostandards and Geoanalytical Research, Volume 40(3), pages 311-332.

Kärenlampi, K., Kontinen, A., Hanski, E., Huhma, H., Lahaye, Y, Krause, J. and Heinig, T.
2020: Age and origin of the Nb-Zr-REE mineralization in the Paleoproterozoic A1-type granitoids at Otanmäki, central Finland. Bulletin of the Geological Society of Finland, Volume 92, pages 39-71.
https://doi.org/ 10.17741/bgsf/92.1.003

Ludwig, K.
2012: User's manual for Isoplot/Ex rev. 3.70: A Geochronological Toolkit for Microsoft Excel. Berkeley Geochronology Center, Berkeley, Special Publication 5, 76 pages.

Magyarosi, Z.
2022: Preliminary investigation of rare earth element mineralization associated with the Fox Harbour Volcanic Belt, southeastern Labrador. *In* Current Research. Government of Newfoundland and Labrador, Department of Industry, Energy and Technology, Geological Survey, Report 22-1, pages 57-83.

Magyarosi, Z. and Rayner, N.
2023: Petrography, geochemistry and geochronology of the REE-mineralized Fox Harbour Volcanic Belt, southeastern Labrador. *In* Current Research. Government of Newfoundland and Labrador, Department of Industry, Energy and Technology, Geological Survey, Report 23-1, pages 47-75.

2024: REE pegmatites and their parent intrusions south of the Fox Harbour Volcanic Belt, southeastern Labrador. *In* Current Research. Government of Newfoundland and Labrador, Department of Industry, Energy and Technology, Geological Survey, Report 24-1, pages 53-78.

2025: REE mineralization in the Port Hope Simpson – St. Lewis area, southeastern Labrador: Mineralogy, geochemistry, geochronology, Sm-Nd isotopes and genetic implications. *In* Targeted Geoscience Initiative 6: Magmatic Ore Systems. *Edited by* W. Bleeker and A-A. Sappin. Geological Survey of Canada.

Miller, R.R.
2015: Pantellerite-hosted rare earth element mineralization in southeast Labrador: The Foxtrot deposit. *In* Symposium on Strategic and Critical Materials Proceedings. *Edited by* G.J. Simandl and M. Neetz. British Columbia Ministry of Energy and Mines, British Columbia Geological Survey, Paper 2015-3, pages 109-117.

Miller, R.R., Heaman, L.M. and Birkett, T.C.
1997: U-Pb zircon age of the Strange Lake peralkaline complex: Implications for Mesoproterozoic peralkaline magmatism in north-central Labrador. Precambrian Research, Volume 81, pages 67-82.

Nunn, G.A.G. and van Nostrand, T.
1996a: Geology of the Kenemich River map area (NTS 13G/SW), Labrador. *In* Current Research. Government of Newfoundland and Labrador, Department of Natural Resources, Geological Survey, Report 96-1, pages 73-83.

1996b: Geology of the Kenemich River map area, Labrador. Map 9634. Government of Newfoundland and Labrador, Department of Natural Resources, Geological Survey, Open File 13G/0048.

Steiger, R.H. and Jäger, E.
1977: Subcommission on geochronology; Convention on the use of decay constants in geo- and cosmochronology. Earth and Planetary Science Letters, Volume 36, pages 359-362.

Stern, R.A.
1997: The GSC Sensitive High Resolution Ion Microprobe (SHRIMP): analytical techniques of zircon U-Th-Pb age determinations and performance evaluation. *In* Radiogenic Age and Isotopic Studies. Report 10, Geological Survey of Canada, Current Research 1997-F, pages 1-31.

Stern, R.A. and Amelin, Y.,
2003. Assessment of errors in SIMS zircon U-Pb geochronology using a natural zircon standard and NIST SRM 610 glass. Chemical Geology, Volume 197, pages 111-146.

Tucker, R. and Gower, C.
1994: A U-Pb geochronological framework for the Pinware terrane, Grenville Province, southeast

Labrador. The Journal of Geology, Volume 102(1), pages 67-78.

van Nostrand, T.
1992: Geology of the Alexis River region, Grenville Province, southeastern Labrador. Government of Newfoundland and Labrador, Department of Mines and Energy, Report 92-3, 27 pages.

van Nostrand, T., Dunphy, D. and Eddy, D.
1992: Geology of the Alexis River region, Grenville Province, southeastern Labrador. *In* Current Research. Government of Newfoundland and Labrador, Department of Mines and Energy, Geological Survey Branch, Report 92-1, pages 399-412.

Wardle, R.J., Gower, C.F., Ryan, B., Nunn, G.A.G., James, D.T. and Kerr, A.
1997: Geological map of Labrador. Government of Newfoundland and Labrador, Department of Natural Resources, Geological Survey, Map 97-07.

Whitney, D.L. and Evans, B.W.
2010: Abbreviations for names of rock-forming minerals. American Mineralogist, Volume 95, pages 185-187.

Wise, M.A., Müller, A. and Simmons, W.B.
2022: A proposed new mineralogical classification system for granitic pegmatites. The Canadian Mineralogist, Volume 60, pages 229-248.